Two-ligand priming mechanism for potentiated phosphoinositide synthesis is an evolutionarily conserved feature of Sec14-like phosphatidylinositol and phosphatidylcholine exchange proteins

Jin Huang[a,†], Ratna Ghosh[a,†], Ashutosh Tripathi[a], Max Lönnfors[a], Pentti Somerharju[b], and Vytas A. Bankaitis[a,c,d,*]

[a]Department of Molecular and Cellular Medicine, College of Medicine, Texas A&M Health Sciences Center, College Station, TX 77843-1114; [b]Faculty of Medicine, Department of Biochemistry and Developmental Biology, University of Helsinki, 00290 Helsinki, Finland; [c]Department of Biochemistry and Biophysics, Texas A&M University, College Station, TX 77843-2128; [d]Department of Chemistry, Texas A&M University, College Station, TX 77840

ABSTRACT Lipid signaling, particularly phosphoinositide signaling, plays a key role in regulating the extreme polarized membrane growth that drives root hair development in plants. The *Arabidopsis AtSFH1* gene encodes a two-domain protein with an amino-terminal Sec14-like phosphatidylinositol transfer protein (PITP) domain linked to a carboxy-terminal nodulin domain. AtSfh1 is critical for promoting the spatially highly organized phosphatidylinositol-4,5-bisphosphate signaling program required for establishment and maintenance of polarized root hair growth. Here we demonstrate that, like the yeast Sec14, the AtSfh1 PITP domain requires both its phosphatidylinositol (PtdIns)- and phosphatidylcholine (PtdCho)-binding properties to stimulate PtdIns-4-phosphate [PtdIns(4)P] synthesis. Moreover, we show that both phospholipid-binding activities are essential for AtSfh1 activity in supporting polarized root hair growth. Finally, we report genetic and biochemical evidence that the two-ligand mechanism for potentiation of PtdIns 4-OH kinase activity is a broadly conserved feature of plant Sec14-nodulin proteins, and that this strategy appeared only late in plant evolution. Taken together, the data indicate that the PtdIns/PtdCho-exchange mechanism for stimulated PtdIns(4)P synthesis either arose independently during evolution in yeast and in higher plants, or a suitable genetic module was introduced to higher plants from a fungal source and subsequently exploited by them.

INTRODUCTION

Phosphoinositide signaling represents a major mechanism by which all eukaryotic cells coordinate cellular responses to both intracellular and extracellular cues with spatial and temporal specificity (Di Paolo and De Camilli, 2006; Bunney and Katan, 2010; Balla, 2013). These lipids are phosphorylated derivatives of their metabolic precursor, phosphatidylinositol (PtdIns), and the chemical diversity of these signaling molecules is simple, as the most complex eukaryotes produce only seven. Yet phosphoinositides regulate literally hundreds

of diverse biological reactions. The mechanisms for how so many biological outcomes derive from such a chemically simple cohort of lipids is incompletely understood. It is in that capacity that members of the Sec14-like phosphatidylinositol transfer protein (PITP) superfamily are emerging as key regulators of specific interfaces between lipid metabolism and PtdIns signaling in diverse cellular processes. Evidence indicates Sec14-like PITPs harness their heterotypic lipid exchange activities to couple stimulated phosphatidylinositol-4-phosphate (PtdIns(4)P) production with the execution of dedicated biological outcomes (Schaaf et al., 2008; Bankaitis et al., 2010). Because Sec14 domains are often found in the context of multidomain proteins, it is an attractive proposition that such an engineering principle reports the physical arrangements of highly integrated signaling units that house both phosphoinositide production and appropriate effector capabilities (Ile et al., 2006; Bankaitis et al., 2010; Ghosh et al., 2015).

In recent years, plants have come to the fore as outstanding model organisms for the study of phosphoinositide biology (Kearns et al., 1998; Qin and Wang, 2002; Monteiro et al., 2005: Yang 2008; Heilmann, 2009; Heilmann and Heilmann, 2015: Munnik and Nielsen, 2011; Boss and Im, 2012; Huang et al., 2016). In that regard, the Sec14-nodulin proteins of higher plants offer a unique opportunity to study mechanisms of function of Sec14 multidomain proteins, and the Sec14-nodulin protein family is being exploited to such ends (Kapranov et al., 2001; Vincent et al., 2005; Huang et al., 2013). This modular arrangement was first discerned when a *Lotus japonicus* 16-kDa protein of unknown function (Nlj16), a polypeptide expressed specifically by the legume in root N$_2$-fixing nodules infected by *Rhizobium* bacteria (hence the term nodulin), was found to be encoded in the genome as a chimeric Sec14-nodulin protein. The free-standing nodulin domain is produced in root nodules at the expense of the full-length Sec14-nodulin because the transcriptional strategy by which this gene is expressed is subject to a dramatic developmental reconfiguration during nodulation (Kapranov et al., 2001). As detailed further here, the expanding library of sequenced genomes emphasizes the vigorous amplification of the Sec14-nodulin gene family in higher plants.

The biological rationale for the physical linkage of Sec14 and nodulin domains and for the developmentally regulated reconfiguration of this genetically encoded modular arrangement is now coming into focus. Functional studies in both *Arabidopsis* and rice demonstrate that at least one member of the family in each case (AtSfh1/Cow1 and OsSndp1, respectively) plays an essential role in establishing and/or maintaining the extreme polarized membrane growth program required for proper root hair biogenesis in its natural plant context (Grierson et al., 1997; Böhme et al., 2004; Vincent et al., 2005; Huang et al., 2013). The *Arabidopsis* AtSfh1 protein offers the most experimentally tractable model for mechanistic dissection of Sec14-nodulin protein function. AtSfh1 supports polarized membrane growth function by establishing and/or maintaining a tip-directed phosphatidylinositol 4,5-bisphosphate (PtdIns(4,5)P$_2$) gradient (Vincent et al., 2005). In that regard, biochemical and genetic evidence identifies the AtSfh1 nodulin domain as a specific PtdIns(4,5)P$_2$-binding module that has the added property of assembling into higher-order homo-oligomers (Ghosh et al., 2015). Evidence suggests that homo-oligomerization of the AtSfh1 nodulin domain and that of other members of the Nlj16-like nodulin domain family is enhanced upon PtdIns(4,5)P$_2$ binding. This property conceptualizes a mechanism for AtSfh1-mediated lateral organization of phosphoinositide pools on membrane surfaces and suggests a high-resolution mechanism for spatial patterning of the lipid sig-

naling program that drives polarized membrane growth (Ghosh et al., 2015).
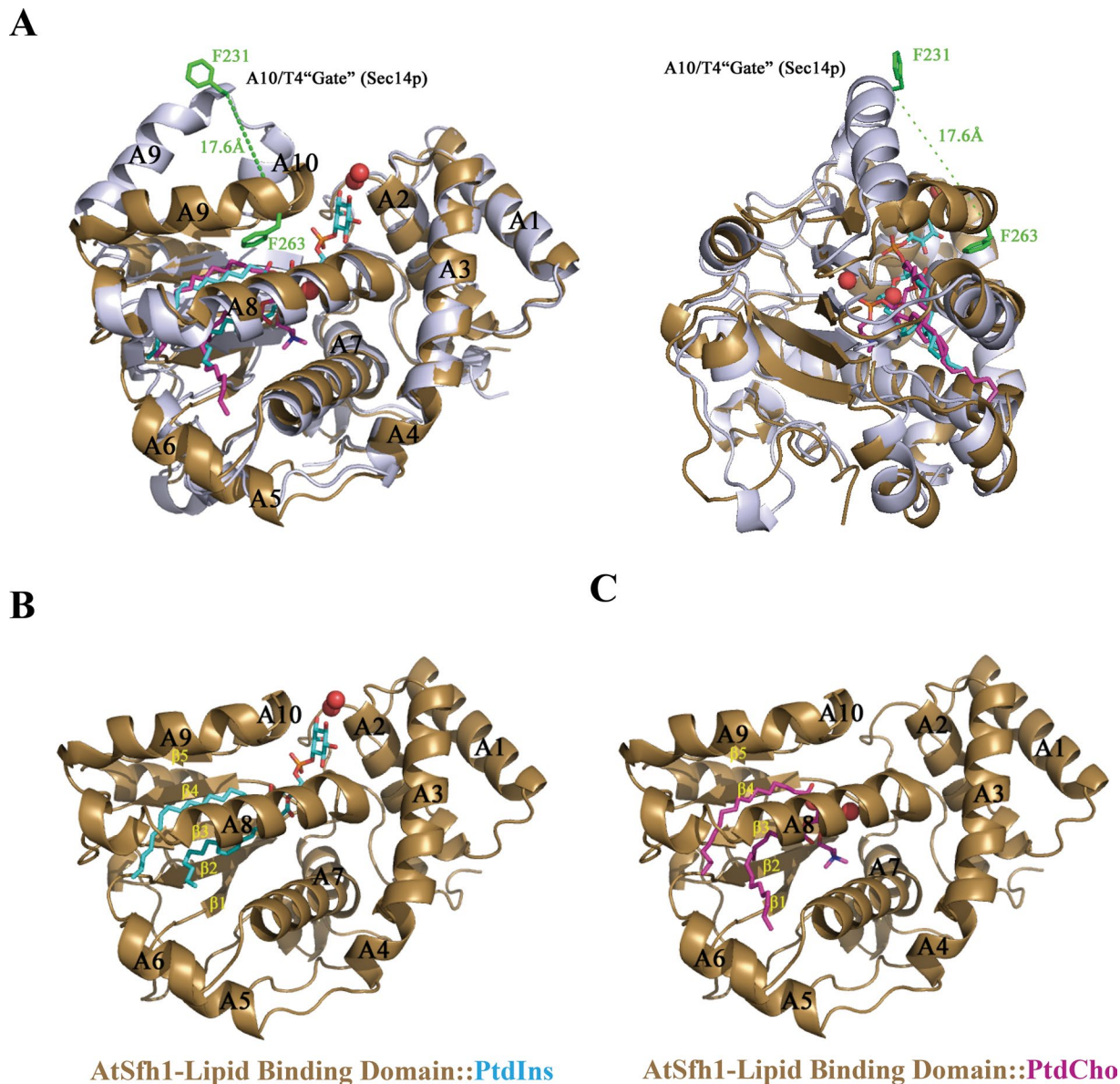
A central feature of current ideas for how AtSfh1 works as a molecule is that the Sec14 domain, which has the capacity to bind both PtdIns and phosphatidylcholine (PtdCho; Vincent et al., 2005), stimulates the activities of PtdIns 4-OH kinases in a manner dependent upon the competitive binding of two distinct lipid molecules. However, whether the AtSfh1 Sec14-domain has the capacity to potentiate phosphoinositide synthesis by PtdIns kinases, whether both PtdIns- and PtdCho-binding activities are required for this activity, and whether such an activity is of functional relevance in its natural biological context remain to be established.

Here we demonstrate that the AtSfh1 Sec14 domain has the intrinsic capacity to stimulate PtdIns(4)P synthesis by PtdIns 4-OH kinases, that this activity requires both the PtdIns- and PtdCho-binding activities of the Sec14 module, and that the PtdIns/PtdCho-exchange mechanism for stimulated PtdIns 4-OH kinase activity is a conserved feature of plant Sec14-nodulin proteins. We also present evidence that Sec14-nodulin proteins arrived at a structural solution for PtdIns- and PtdCho-binding that essentially replicates the one displayed by the yeast Sec14 and Sfh1 proteins. This convergence is striking, given that Sec14-nodulin proteins are expressed by only the most evolutionarily advanced plants and that the PtdIns- and PtdCho-binding elements of lower-plant Sec14-like proteins are structurally and functionally degenerate relative to those of the yeast Sec14 PtdIns/PtdCho-transfer proteins. The collective data indicate that the two-ligand PtdIns/PtdCho-exchange mechanism is conserved in Sec14-like PtdIns/PtdCho-transfer proteins of organisms separated by vast evolutionary distances. The data also raise interesting questions regarding whether this conservation reflects convergent evolution or exploitation of lateral gene transfer.

RESULTS

Homology model of the AtSfh1 Sec14 domain

Among the 31 Sec14-like proteins in *Arabidopsis*, the 12 highest-scoring proteins belong to the Sec14-nodulin family. The Sec14 domains of these Sec14-nodulin proteins share 40–60% primary sequence identity to yeast Sec14. The AtSfh1 Sec14 domain, which we refer to as the lipid-binding domain (LBD), shares 62% primary sequence identity with yeast Sec14. This extensive sequence homology between the yeast Sec14 and Sfh1 proteins and the AtSfh1 LBD provided a detailed template for construction of a three-dimensional (3D) AtSfh1-LBD homology model based on high-resolution crystal structures solved for the PtdIns- and PtdCho-bound forms of Sfh1 (Schaaf et al., 2008). That the model showed a high sequence-structure compatibility score of 0.68 reflected the strong structural conservation between the AtSfh1 LBD and Sfh1. It also inspired confidence that the homology model is a structurally accurate representation. The AtSfh1-PtdIns/PtdCho homology models were further optimized in molecular dynamics (MD) simulations by subjecting them to energy minimization and a series of equilibration steps followed by a 10-ns production run. Comparisons of the corresponding root mean square deviation and root mean square fluctuation (RMSF) values between the C-α atoms of the initial homology models calculated for the PtdIns and PtdCho-bound AtSfh1 LBD models and the corresponding post–MD simulation complexes reported C-α RMSF values within a range of 1.5–2.5 Å (Figure 1A). Those data indicate that PdtIns/PtdCho binding to the LBD further stabilized the closed AtSfh1 conformer and that the associated ligand-induced conformational changes observed were within reasonable limits.

A

F231
A10/T4"Gate" (Sec14p)
17.6Å
A9
A9
A10
A2
A1
F263
A3
A8
A7
A6
A4
A5

A10/T4"Gate" (Sec14p)
F231
17.6Å
F263

B

A9
A10
A2
β5
A1
β4
A3
β3
A8
β2
A7
β1
A6
A4
A5

C

A9
A10
A2
β5
A1
β4
A3
β3
A8
β2
A7
β1
A6
A4
A5

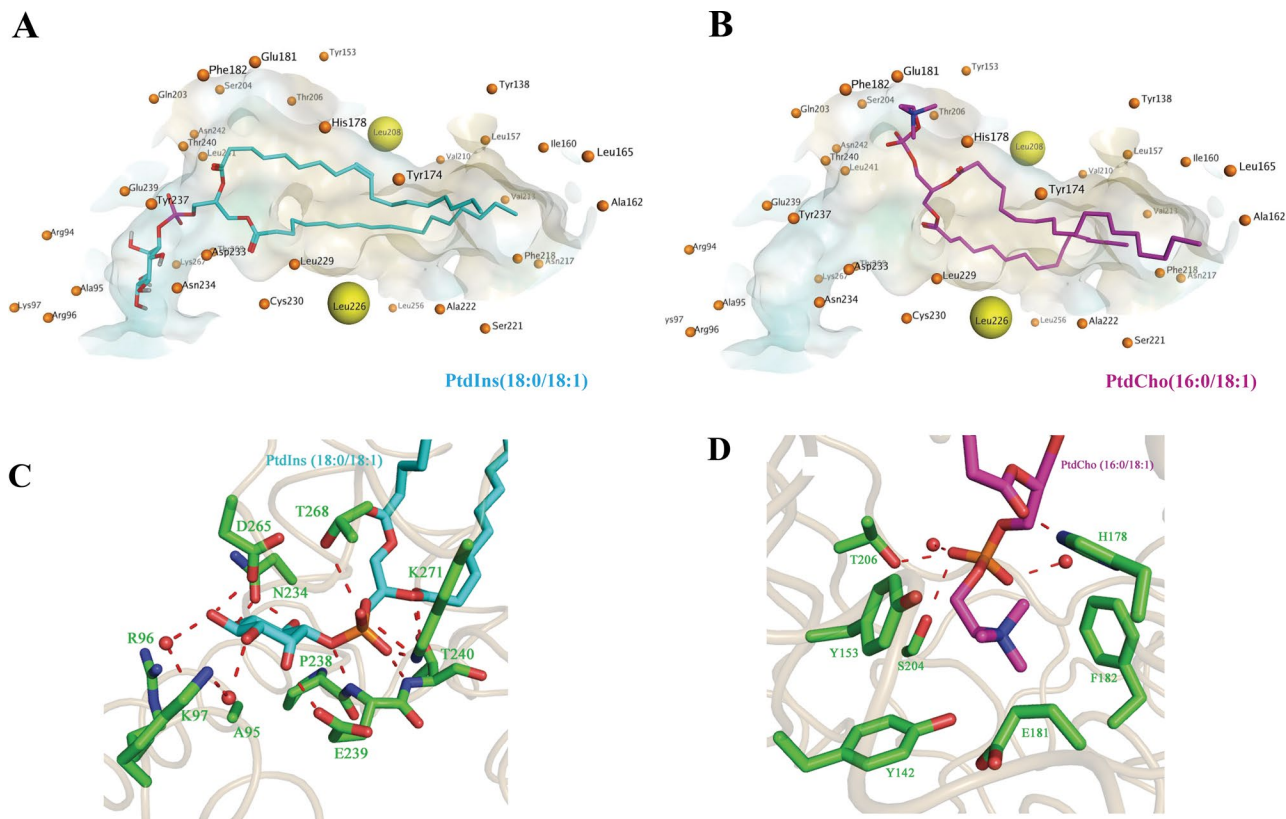**AtSfh1-Lipid Binding Domain::PtdIns**   **AtSfh1-Lipid Binding Domain::PtdCho**

FIGURE 1: Three-dimensional homology model for the AtSfh1 Sec14 domain. (A) Closed conformation of AtSfh1::PtdIns/PtdCho complex (gold) superimposed on the open structure of Sec14 (blue gray). The 17.6-Å displacement of the A_9/A_{10} helical gate between the open and closed conformers is shown by a dashed line between the α-carbons of F_{231} in the Sec14 open conformer and F_{263} located at the C-terminus of helix A_9 in the closed AtSfh1::PtdIns/PtdCho conformer. PtdIns and PtdCho are rendered in blue and magenta, respectively. AtSf1h::PtdIns (B) and AtSfh1::PtdCho (C) complexes are oriented to highlight the difference in the inositol and choline head-group binding sites. Red spheres represent ordered water molecules that coordinate the phosphate moiety of each phospholipid.

The homology models further predicted that, like Sec14 (Sha et al., 1998; Schaaf et al., 2008), the first four α-helices of the AtSfh1-LBD fold into a tripod motif, whereas the phospholipid-binding pocket floor is formed by a five-stranded β-sheet capped by three α-helices. The AtSfh1-LBD structural element that gates access to the phospholipid-binding pocket comprises a single α-helix (A_9), and this gating substructure shows a 17.6-Å displacement from helix A_8 when the protein is modeled in an open conformation (Figure 1A). In the closed phospholipid-bound conformer, helix A_9 and A_{10} interactions with helix A_8 and β-strand B_5 are projected to be stabilized by hydrophobic contacts and interactions with the *sn-1* acyl chain of bound phospholipid (Figure 1, B and C).

AtSfh1-LBD phospholipid-binding motifs

As was observed in the phospholipid-bound Sfh1 crystal structures, the PtdCho head group is projected to be buried deep within the AtSfh1-LBD hydrophobic cavity, whereas the PtdIns head group is positioned near the protein surface and is oriented toward the "mouth" of the hydrophobic phospholipid-binding pocket (Figure 1, B and C). The 3D models of PtdIns- and PtdCho-bound AtSfh1-LBD forms display a highly conserved set of hydrophobic residues that lie within 4 Å of the fatty acyl chains. The structural elements that coordinate PtdIns and PtdCho head-group binding are similarly conserved with respect to those identified in Sec14 and Sfh1 crystal structures (Figure 2, A and B). Molecular dynamic simulation studies further projected that PtdIns and PtdCho binding is stabilized within

FIGURE 2: Structural models of AtSfh1-lipid binding domain complexed with PtdIns and PtdCho. Residues within 4 Å of bound 18:0/18:1 PtdIns (A) and 16:0/18:1 PtdCho (B) are represented as orange spheres and are conserved relative to the corresponding residues in yeast Sfh1. Yellow spheres highlight residues where incorporation of bulky side chains pinches PtdIns and PtdCho acyl-chain binding space in the yeast Sec14 and Sfh1 PITPs (Schaaf *et al.*, 2008). Residues involved in the stabilization of the inositol ring, choline head group, phosphate moiety, and glycerol backbone of 18:0/18:1PtdIns (C) and 16:0/18:1 PtdCho (D) are shown. Red spheres represent ordered water molecules that coordinate the phosphate moiety of each phospholipid. Potential hydrogen bonds spanning distances of <2.5–3.0 Å are depicted by dashed lines.

the AtSfh1 Sec14 fold by distinct networks of hydrogen bond and H_2O bridges to critical residues in the respective head-group binding sites. The AtSfh1-LBD::PtdIns complex is stabilized via a network of hydrogen bond interactions (Supplemental Figure S1, A and B). Molecular dynamics simulations indicated AtSfh1-LBD residues R_{96}, K_{97}, N_{234}, E_{239}, and D_{265} engage the Ins ring, whereas residues P_{238}, T_{268}, and K_{271} coordinate the PtdIns phosphate moiety via hydrogen bonds—a PtdIns head-group coordination strategy that essentially recapitulates those solved for Sfh1 and Sec14 by crystallography (Figure 2C; Phillips *et al.*, 1999: Schaaf *et al.*, 2008).

In the AtSfh1-LBD::PtdCho model, the choline head group is predicted to make hydrophobic contacts between residues Tyr_{142}, Tyr_{153}, and Phe_{182}, whereas the PtdCho phosphate oxygen engages residues Tyr_{142}, Ser_{204}, and Thr_{206} via a hydrogen bond network that further stabilizes the phospholipid::protein complex (Supplemental Figure S1, C and D). The side-chain –OH groups of AtSfh1 residues S_{204} and T_{206} are projected to be particularly important for coordinating the PtdCho head-group phosphate (Figure 2D).

The structural modeling experiments further identified AtSfh1 L_{208} and L_{226} as residues whose side chains sandwich the acyl chains in the heart of the LBD hydrophobic cavity (represented as yellow spheres in Figure 2, A and B). The corresponding residues in Sfh1 (L_{179} and I_{196}) are similarly positioned relative to acyl chain space in the high-resolution Sfh1::PtdCho and Sfh1::PtdIns crystal structures.

Missense substitution of those residues with amino acids harboring bulky side chains (e.g., Sec14^{M177W,V194W} and Sfh1^{L179W,I196W}, respectively) is incompatible with PtdIns and PtdCho acyl chain access to the hydrophobic pocket—representing so-called "pinch-close" mutants (Schaaf *et al.*, 2008). The cognate substitutions in the AtSfh1 LBD are similarly predicted to sterically clash with both PtdIns and PtdCho binding.

Mutant AtSfh1 LBDs with specific phospholipid-binding/transfer defects

The AtSfh1 LBD homology model identified residues R_{96} and K_{97} as establishing direct hydrogen bond interactions with the PtdIns inositol head group and residues K_{271} and T_{268} in coordination of the PtdIns phosphate moiety by hydrogen bonding. Thus, AtSfh1 LBDs carrying $K_{97}A,K_{271}A$ or $R_{96}A,T_{268}D$ double missense substitution were generated with the expectation that those mutant proteins would show selective defects in PtdIns binding/transfer. By contrast, the AtSfh1 LBD is predicted to coordinate the phosphate moiety of bound PtdCho via hydrogen bond interactions with the side-chain –OH groups of PtdCho barcode residues S_{204} and T_{206}. Using functional analyses of Sec14 and Sfh1 as precedent (Schaaf *et al.*, 2008), we converted each of those two residues to Ile with the expectation that the double-mutant LBD would show selective defects in PtdCho binding/transfer.
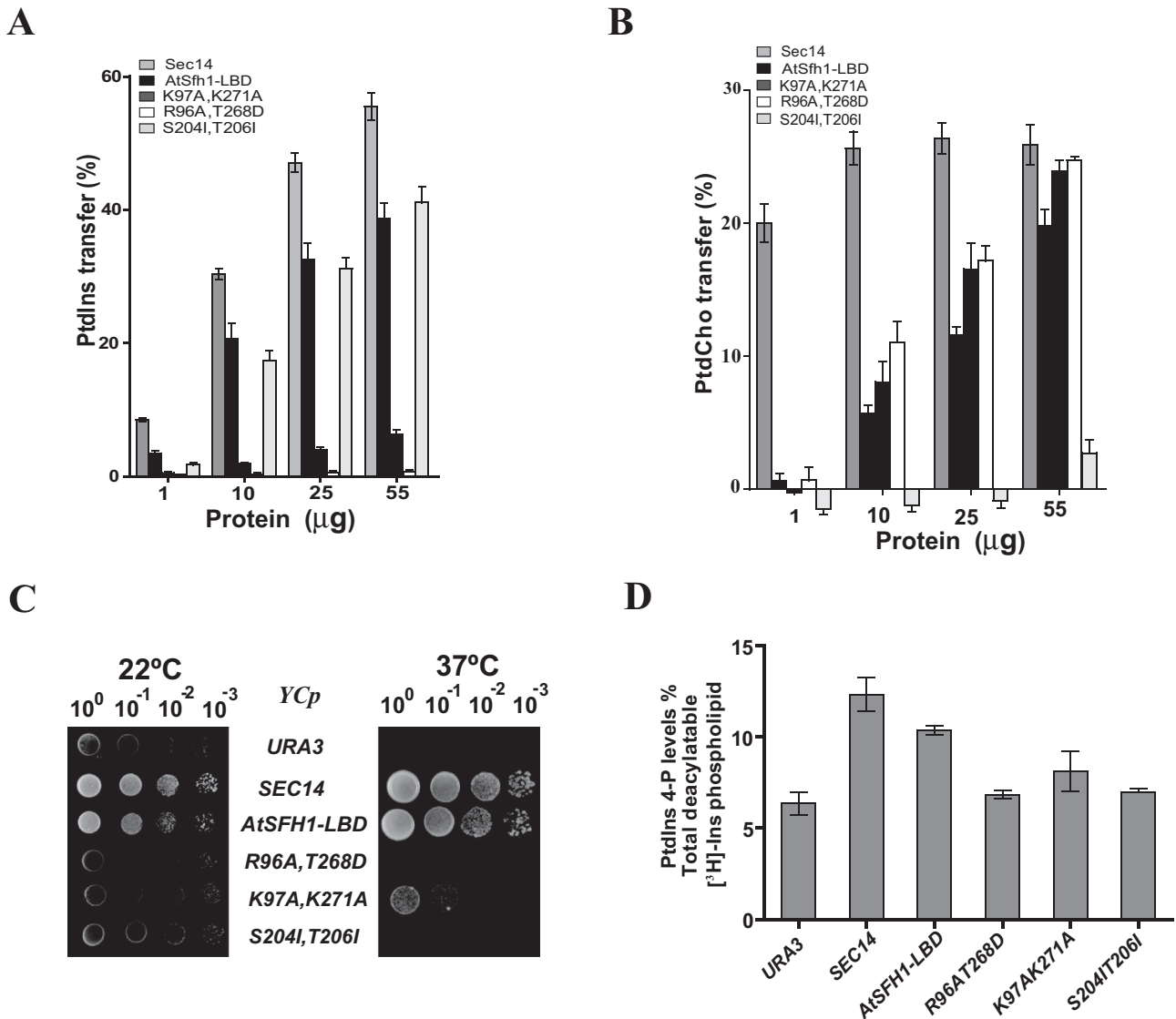
FIGURE 3: PtdIns- and PtdCho-binding-defective AtSfh1 Sec14 LBDs fail to stimulate PtdIns 4-OH kinase in cells. Results from PtdIns- (A) and PtdCho-transfer (B) assays with purified histidine-tagged proteins of WT AtSfh1-LBD and its mutant versions AtSfh1-LBD^{R96A,T268D}, AtSfh1-LBD^{K97A,K271A}, and AtSfh1-LBD^{S204I,T206I}, respectively (identification legend at top). Purified yeast Sec14 served as positive control in these assays. All assays were performed in at least triplicate. The PtdIns- and PtdCho-transfer assays used increasing amounts of purified recombinant proteins as indicated at the bottom. Representative data from four different experiments ($n = 4$). (C) Yeast complementation assays. Isogenic *sec14-1*^{ts} yeast strains carrying the indicated yeast centromeric (YCp) plasmids were spotted in 10-fold dilution series onto agar plates and incubated at the restrictive temperature of 37°C. YCp(*URA3*) and YCp(*SEC14*) derivatives served as negative and positive controls. (D) Quantification of bulk cellular PtdIns(4)phosphate in isogenic derivatives of the *sec14-1*^{ts} *sac1*Δ yeast strain CTY100 (carrying designated YCp plasmids) radiolabeled for at least six generations in minimal medium supplemented with [³H]inositol (20 μCi/ml). YCp(*URA3*) and YCp(*SEC14*) derivatives served as negative and positive controls, respectively. PtdIns(4)P levels are increased in YCp(*SEC14*) and YCp(*AtSFH1-LBD*) derivative strains relative to YCp(*URA3*) negative control (pairwise *t* test, $p < 0.0001$; $n = 5$) but significantly reduced in YCp(*Atsfh1*^{K97A,K271A}-*LBD*), YCp(*Atsfh1*^{R96A,T268D}-*LBD*), and YCp(*Atsfh1*^{S204I,T206I}-*LBD*) relative to YCp(*AtSFH1-LBD*) and YCp(*SEC14*). Pairwise *t*-test analyses also showed that the YCp(*Atsfh1*^{K97A,K271A}-*LBD*), YCp(*Atsfh1*^{R96A,T268D}-*LBD*), and YCp(*Atsfh1*^{S204I,T206I}-*LBD*) conditions all showed statistically significant reductions in PtdIns(4)P levels relative to the YCp(*AtSFH1-LBD*) positive control ($p = 0.0022$, $p < 0.0001$, and $p < 0.0001$, respectively; $n = 5$). In contrast, pairwise *t*-test analyses showed that, relative to the YCp(*URA3*) negative control, only the YCp(*Atsfh1*^{K97A,K271A}-*LBD*) condition showed a significant increase in PtdIns(4)P levels ($p = 0.0134$; $n = 5$). The YCp(*Atsfh1*^{R96A,T268D}-*LBD*) and YCp(*Atsfh1*^{S204I,T206I}-*LBD*) conditions did not show significant differences ($p > 0.09$; $n = 5$).

The mutant AtSfh1 LBDs were purified as recombinant proteins, and their respective PtdIns- and PtdCho-transfer activities were analyzed in vitro. Sec14 and wild-type (WT) AtSfh1 both displayed robust concentration-dependent PtdIns transfer activity, but the

AtSfh1 LBDs carrying missense substitutions in amino acids projected to coordinate the PtdIns head group showed dramatic defects in this specific activity. Whereas the AtSfh1^{K97A,K271A} LBD was only ~10% as active as WT AtSfh1 LBD for PtdIns transfer, the

AtSfh1[R96A,T268D] LBD showed essentially no activity in this assay (Figure 3A). That these proteins were selectively defective in PtdIns binding/transfer and not simply malfolded was demonstrated by the fact that both AtSfh1[K97A,K271A] and AtSfh1[R96A,T268D] LBDs remained uncompromised for PtdCho-transfer activity (Figure 3B). In contrast, the AtSfh1[S204I,T206I] LBD was severely impaired (~90% reduced) for PtdCho transfer relative to Sec14 and the WT AtSfh1 LBD but exhibited no such diminution in PtdIns-transfer activity (Figure 3, A and B). Those results established that the AtSfh1[S204I,T206I] LBD was a structurally intact protein with a specific defect in PtdCho binding/transfer.

Mutant AtSfh1 LBDs fail as functional surrogates for Sec14 activity in yeast

That the AtSfh1 LBD is able to discharge Sec14-like activities in stimulating PtdIns 4-OH kinase activities in yeast was suggested by the fact that its expression rescued growth of *sec14-1[ts]* mutants at restrictive temperatures and, even more dramatically, rescued the unconditional lethality associated with *sec14Δ* alleles (Vincent *et al.*, 2005). If the mechanism by which Sec14 stimulates PtdIns 4-OH kinase activities is conserved across wide evolutionary distances, AtSfh1 LBDs deficient in either PtdIns or PtdCho binding should be incapable of stimulating PtdIns(4)P synthesis and therefore incapable of serving as functional Sec14 surrogates in yeast. Consistent with this prediction, whereas Sec14 or AtSfh1 LBD expression efficiently rescued *sec14-1[ts]* growth defects at the restrictive temperature of 37°C, neither expression of the AtSfh1[R96A,T268D] LBD nor that of the AtSfh1[S204I,T206I] LBD was able to do so (Figure 3C). By contrast, expression of AtSfh1[K97A,K271A] LBD, that is, the mutant LBD with partial defects in PtdIns-transfer activity, retained some activity in this bioassay.

Mutant AtSfh1 LBDs fail to stimulate PtdIns 4-OH kinase activities in yeast

The functional readout of biologically sufficient PtdIns- and PtdCho-transfer activity of the AtSfh1 LBD is predicted to be stimulation of phosphoinositide synthesis (Vincent *et al.*, 2005; Ghosh *et al.*, 2015). Impaired PtdIns- or PtdCho-transfer activities of the mutant proteins were therefore anticipated to have deleterious effects on their ability to stimulate phosphoinositide synthesis, particularly PtdIns 4-OH phosphate synthesis, in vivo. This expectation was verified by experiments in which the effects of AtSfh1[R96A,T268D] and AtSfh1[S204I,T206I] LBD expression on PtdIns(4)P synthesis were analyzed in a yeast context. In those experiments, a *sec14-1[ts] sac1* strain was used for the analyses. This mutant strain is deficient in the major pathway for PtdIns(4)P degradation (*sac1*) and, as a result, retains viability in the absence of the normally essential Sec14 protein (Cleves *et al.*, 1989; Guo *et al.*, 1999; Rivas *et al.*, 1999). Owing to its Sac1 phosphatase deficiency, the *sac1*-null mutant accumulates PtdIns(4)P to levels in large excess of those exhibited by WT cells, thereby simplifying PtdIns(4)P quantification and restricting any observed changes to alterations in PtdIns(4)P production rather than in degradation rate.

Steady-state *myo*-[2-^{3}H] inositol radiolabeling experiments demonstrated that, whereas expression of the WT AtSfh1-LBD elicited significant elevations in PtdIns(4)P and PtdIns(4,5)P_2 levels in the Sec14-deficient yeast strain compared with basal control (Figure 3D), expression of neither the PtdIns- nor the PtdCho-binding-defective mutant AtSfh1 LBDs was able to do so. Of the two PtdIns-binding-defective mutants, AtSfh1[K97A,K271A]-LBD expression was slightly more efficient in elevating PtdIns(4)P levels than was expression of the AtSfh1[R96A,T238D]-LBD (Figure 3D). Those in vivo results were consistent with the biochemical activities of the two mutant proteins in PtdIns- and PtdCho-transfer assays. That is, the

AtSfh1[K97A,K271A]-LBD was partially defective for PtdIns-binding activity in vitro and stimulation of PtdIns(4)P synthesis in vivo, whereas the AtSfh1[R96A,T238D]-LBD scored as a null in both sets of assays. Taken together, those independent sets of analyses establish that, whereas both PtdIns- and PtdCho-binding activities were necessary for stimulation of PtdIns 4-OH kinases in a yeast model, neither activity was by itself sufficient.

AtSfh1 PtdIns- and PtdCho-binding mutants show deranged root hair biogenesis

The availability of mutant AtSfh1 Sec14 domains with specific defects in PtdIns- or PtdCho-exchange activities afforded an opportunity to determine whether these Sec14 domain–associated lipid-binding activities are essential for AtSfh1 function in root hair biogenesis. Moreover, these mutants simultaneously enabled a direct test of whether the two-ligand mechanism for Sec14 function operates in a higher eukaryote. To those ends, we reconstituted *Atsfh1*-null plants for expression of mutant *Atsfh1* transgenes expressing proteins with specific PtdIns- and PtdCho-binding defects. The biological properties of the PtdIns-binding-defective *Atsfh1[R96A,T238D]* and *Atsfh1[K97A,K271A]* and the PtdCho-binding-defective *Atsfh1[S204I,T206I]* transgenes were then examined. Whereas the transgenes were expressed ectopically, their expression remained under control of natural *AtSFH1* promoter and terminator sequences. T3 homozygous transgenic plant lines were generated and subsequently analyzed by environmental scanning electron microscopy (ESEM) for complementation of *Atsfh1[0/0]* short–root hair phenotypes. Whereas an *AtSFH1^{+}* transgene rescued the *Atsfh1[0/0]* null condition, none of the *Atsfh1* transgenes expressing proteins with mutant Sec14 domains complemented the root hair phenotypes of *Atsfh1[0/0]* plants when expressed in that genetic background (Figure 4A).

We examined the root hair phenotypes in greater detail by quantifying root hair lengths and the frequencies of double root hairs (root hairs with two growing tips), triple root hairs (three growing tips), and notched root hairs of homozygous T3 seedlings and comparing the values with those recorded for WT and null controls (Figure 4B and Supplemental Table S1). As previously reported, the average root hair lengths of *Atsfh1[0/0]* mutants were only one-third the length of those of age-matched wild-type seedlings (Vincent *et al.*, 2005). Reconstitution of *Atsfh1[0/0]* plants with the *AtSfh1[K97A,K271A]* and *AtSfh1[R96A,T268D]* transgenes yielded seedlings with root hair lengths of 67.53 ± 39.74 and 38.75 ± 28.92 µm, respectively. Those values were in agreement with the biochemical and yeast functional rescue data described earlier, which identified AtSfh1[K97AK271A] as a functional hypomorph and AtSfh1[R96AT268D] as a biologically inactive protein. The PtdCho-binding-defective *Atsfh1[S204I,T206I]* similarly scored as a functional null allele in this biological context, as the root hair phenotype of *Atsfh1[0/0]* seedlings was indifferent to expression of this mutant transgene. All three mutant plant lines (*Atsfh1[K97A,K271A]*, *Atsfh1[R96A,T268D]*, and *Atsfh1[S204I,T206I]*) showed similarly increased frequencies of double root hairs relative to wild-type controls. Triple root hairs were also evident for the AtSfh1[K97A,K271A] lines (Supplemental Table S1). Other than elaboration of the signature *Atsfh1* root hair phenotypes, all the mutant transgenic lines were otherwise normal and fertile. All of the *Atsfh* proteins analyzed were stable when expressed in cells (unpublished data).

AtSfh1 PtdIns- and PtdCho-binding mutants lose tip-directed PtdIns(4,5)P_2 gradients

The loss of polarized tip growth in *Atsfh1[0/0]* root hairs is a consequence of a wholesale collapse of the striking tip-directed PtdIns(4,5)P_2 gradient (Vincent *et al.*, 2005; Ghosh *et al.*, 2015), and this
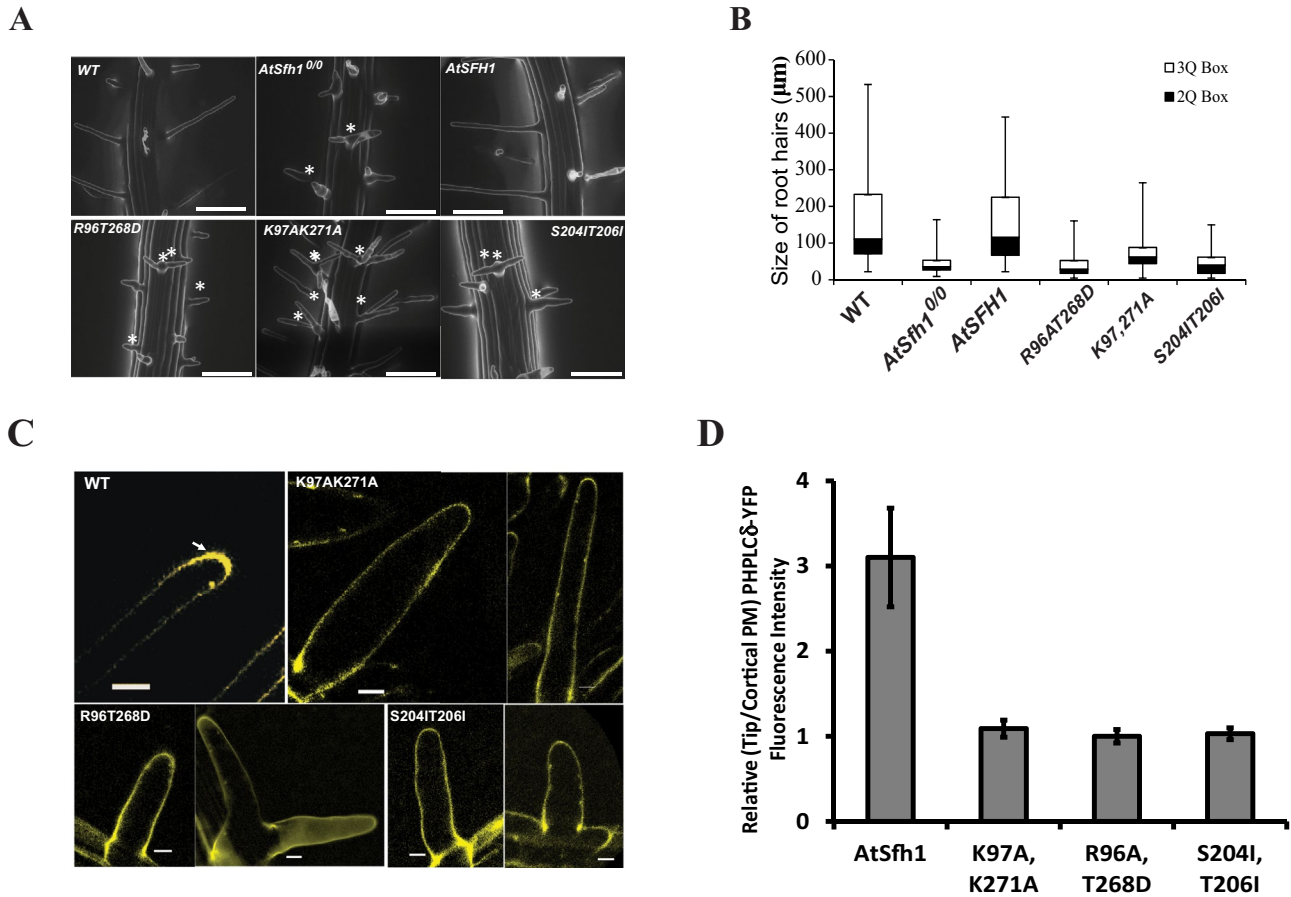
FIGURE 4: Root hair properties of plants expressing AtSfh1 proteins with mutant Sec14 LBDs. (A) High-resolution ESEM images of root hairs of 3-d-old seedlings from WT, $Atsfh1^{0/0}$, and T_3 seedlings of $AtSfh1^{0/0}$ plants expressing ectopic copies of $AtSFH1$ and indicated $Atsfh1$ mutant transgenes. Bars, 300 µm. The single-, double-, and triple-tip-growing root hairs are highlighted by asterisks. (B) Box-and-whisker representation of the root hair lengths observed for 3-d-old seedlings of WT, $AtSfh1^{0/0}$, and T_3 seedlings of $AtSfh1^{0/0}$ plants expressing ectopic copies of $AtSFH1$ and indicated $Atsfh1$ mutant transgenes. The 2Q (black) and 3Q (white) boxes represent the second and third quartiles of the data set, respectively. The whiskers span the first quartile, from the second quartile box down to the minimum, and the fourth quartile from the third quartile box up to the maximum. Pairwise t-test analyses indicated that root hair lengths were significantly increased in the $Atsfh1^{0/0}$ plants expressing an ectopic copy of the $AtSFH1$ transgene relative to $Atsfh1^{0/0}$ plants and $Atsfh1^{0/0}$ plants expressing the indicated mutant transgenes ($p < 0.0001$; $n \leq 155$). (C) Loss of tip-directed PtdIns(4,5)P$_2$ gradients in $Atsfh1^{0/0}$ plants expressing the indicated mutant $Atsfh1$ transgenes. PtdIns(4,5)P$_2$ distribution was visualized as PHPLCδ1-YFP fluorescence in 3-d-old $Atsfh1^{0/0}$ seedlings. PtdIns(4,5)P$_2$ distribution is shown for single and double growing root tips of $Atsfh1^{R96A,T268D}$ and $Atsfh1^{S204I,T206I}$ seedlings. The tip-directed PtdIns(4,5)P$_2$ accumulation is highlighted by an arrow. Scale bar: 10µm. (D) Quantitative plot of the relative intensities of PH$_{PLC}\delta_1$-YFP fluorescence at the tip vs. cortical PM. The relative values were calculated from average maximum line scan intensities perpendicular across tip and cortical PMs taken at three different positions from root hair images collected for each plant type indicated at the bottom of the plot (three root hairs analyzed per genotype). Pairwise t-test analyses indicated that the PHPLCδ1-YFP fluorescence at the tip vs. cortical PM was significantly increased in the $Atsfh1^{0/0}$ plants expressing an ectopic copy of the $AtSFH1$ transgene relative to $Atsfh1^{0/0}$ plants expressing indicated mutant transgenes ($p < 0.02$; $n = 3$).

gradient is a cardinal feature of growing root hairs (Braun *et al.*, 1999; Preuss *et al.*, 2006; Kusano *et al.*, 2008). Because AtSfh1 Sec14 domains with specific PtdIns- or PtdCho-binding defects are defective in stimulation of PtdIns(4)P synthesis, we anticipated that the mutant proteins would be unable to support generation and/or maintenance of tip-directed PtdIns(4,5)P$_2$ gradients in growing root hairs. Whereas $Atsfh1^{0/0}$ root hairs reconstituted for AtSfh1 expression recovered a strong tip-focused PtdIns(4,5)P$_2$ gradient, as assessed by imaging the plasma membrane (PM) distribution of a PtdIns(4,5)P$_2$-specific fluorescent reporter (PLCδ1-PH domain tagged with yellow fluorescent protein [YFP]), the tip-directed PtdIns(4,5)P$_2$ gradients were not apparent in root hairs producing

$AtSfh1^{K97A,271A}$, $AtSfh1^{R96A,T268D}$, or $AtSfh1^{S204I,T206I}$ as sole sources of AtSfh1 activity (Figure 4C).

To quantify tip-directed PtdIns(4,5)P$_2$ gradient status in the mutant root hairs, we drew perpendicular line scans across tip and cortical membranes at three different positions for each TIFF image file presented in Figure 4C using ImageJ after applying background correction to all of the images. The maximum pixel intensities recorded across each set of line scans were averaged for tip PM to cortical PM. The relative intensities of PH$_{PLC}\delta_1$-YFP fluorescence at the tip PM versus cortical PM were subsequently calculated to produce tip PM/cortical PM fluorescence intensity ratios. Those ratios were taken as quantitative estimates of tip-directed
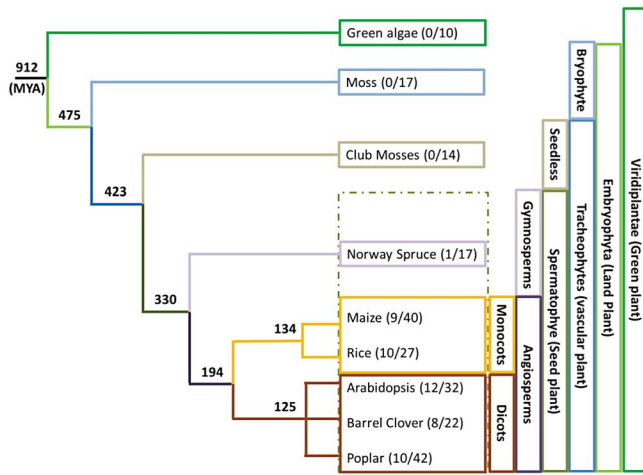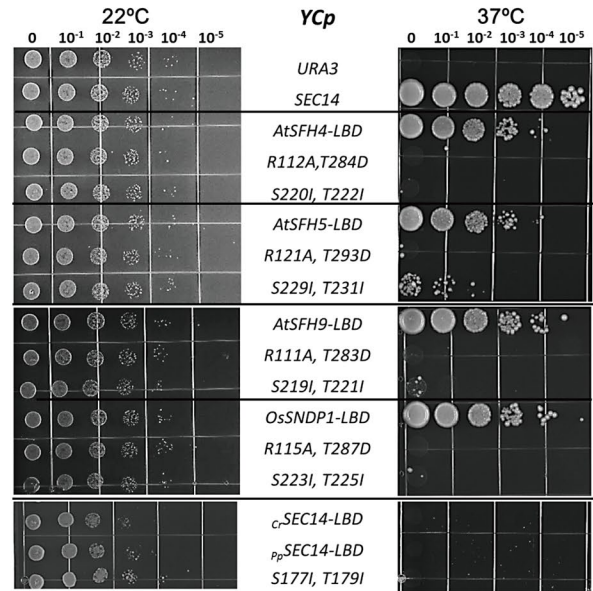
FIGURE 5: Functional requirement for intact Sec14-LBD PtdIns- and PtdCho-binding barcodes is a conserved property of Sec14-nodulin proteins. (A) Distribution of Sec14-nodulin proteins throughout the plant kingdom. BlastP searches were run against the National Center for Biotechnology Information (www.ncbi.nlm.nih.gov/), GreenPhyl (www.greenphyl.org/cgi-bin/index.cgi), and Phytozome (phytozome.jgi.doe.gov/pz/portal.html) databases using the yeast Sec14 as query primary sequence. Confirmed Sec14 homologues were then screened for nodulin domains using the *Lotus japonicus* Nlj16 as query primary sequence and BlastP as the search tool (default parameters; BlastP cutoff value = hit score of 40). Plant species analyzed are indicated, and numbers in parentheses indicate total Sec14-nodulins vs. total Sec14-like proteins produced by the indicated plant species. Left, taxonomic hierarchy of the plant species surveyed. (B) Yeast complementation assays. Isogenic *sec14-1*[ts] yeast strains carrying yeast centromeric (YCp) plasmids expressing the indicated WT and mutant LBDs were spotted in 10-fold dilution series onto agar plates and incubated at the restrictive temperature of 37°C. YCp(*URA3*) and YCp(*SEC14*) derivatives served as negative and positive controls, respectively.

PtdIns(4,5)P$_2$ gradients. In the WT case, the tip PM/cortical PM intensity ratio was 3.10 ± 0.58 (Figure 4D), a value in excellent agreement with previous ratiometric imaging measurements, which reported threefold PtdIns(4,5)P$_2$ enrichments per unit tip PM area relative to unit cortical PM area in growing root hairs of WT *Arabidopsis* seedlings (Vincent *et al.*, 2005; Ghosh *et al.*, 2015). AtSfh1-deficient root hairs reconstituted with AtSfh1[K97A,K271A] protein exhibited a tip PM/cortical PM intensity ratio of 1.14 ± 0.16, signifying collapse of the tip-directed PtdIns(4,5)P$_2$ gradient (Figure 4D). Analyses of AtSfh1-deficient root hairs reconstituted with functionally null AtSfh1[R96A,T268D] and AtSfh1[S204I,T206I] polypeptides yielded similar results (tip PM/cortical PM intensity ratios of 0.94 ± 0.12 and 0.99 ± 0.11; Figure 4D).

Conserved PtdIns- and PtdCho-binding barcodes appear late in plant evolution

The physical joining of Sec14 domains to Njl16-like nodulin domains is a general arrangement, as all described Nlj16-like domains are genetically encoded as C-terminal fusions to Sec14-domains (Kapranov *et al.*, 2001; Vincent *et al.*, 2005; Huang *et al.*, 2013). Phylogenetic analyses show that, whereas the Sec14 domain is conserved throughout the plant kingdom from algae to flowering plants, the Sec14-nodulin arrangement is found only in the most evolutionarily advanced plants. Structural genes encoding Sec14-nodulins are abundantly evident in genomes of flowering plants such as *Arabidopsis*, *Lotus*, *Oryza* (rice), *Maize* (corn), and *Medicago* (barrel clover). All of these plant species harbor at least 10 distinct structural genes encoding Sec14-nodulin proteins (Figure 5A). By

contrast, that modular two-domain arrangement was sparse in gymnosperms (Norway spruce), and we were unable to identify obvious Sec14-nodulin structural genes in club mosses, ferns, or more primitive phyla. Thus, the Sec14-nodulin configuration appeared late in plant phylogeny but was then conserved throughout the most evolutionarily advanced plant species and vigorously amplified by them.

Not only have higher plants conserved the Sec14-nodulin arrangement but, in addition, the structural elements that govern the PtdIns- and PtdCho-binding properties of their corresponding Sec14 domains are also well preserved within this group. Linear primary sequence depictions of the sets of residues that assemble in space to coordinate PtdIns and PtdCho head-group binding by Sec14, Sfh1, and AtSfh1 define the PtdIns- and PtdCho-binding barcodes for these respective proteins. As detailed in Supplemental Figure S2, both PtdIns- and PtdCho-binding barcodes are highly conserved throughout the *Arabidopsis* Sec14-nodulin protein family and in the AtSfh1 orthologues of other flowering plants. Of interest, those barcodes are nearly identical to those of yeast Sec14 and Sfh1. By contrast, the PtdIns- and PtdCho-binding barcodes of Sec14-like proteins of gymnosperms and lower plants, such as club mosses, mosses, and algae, are degenerate relative to the corresponding phospholipid-binding barcodes of the yeast PITPs (Supplemental Figure S2).

Two-ligand binding mechanism for stimulating PtdIns(4)P synthesis is a general property of Sec14-nodulin proteins

The conservation of PtdIns- and PtdCho-binding barcodes in the Sec14-nodulin family suggested that, as demonstrated here for
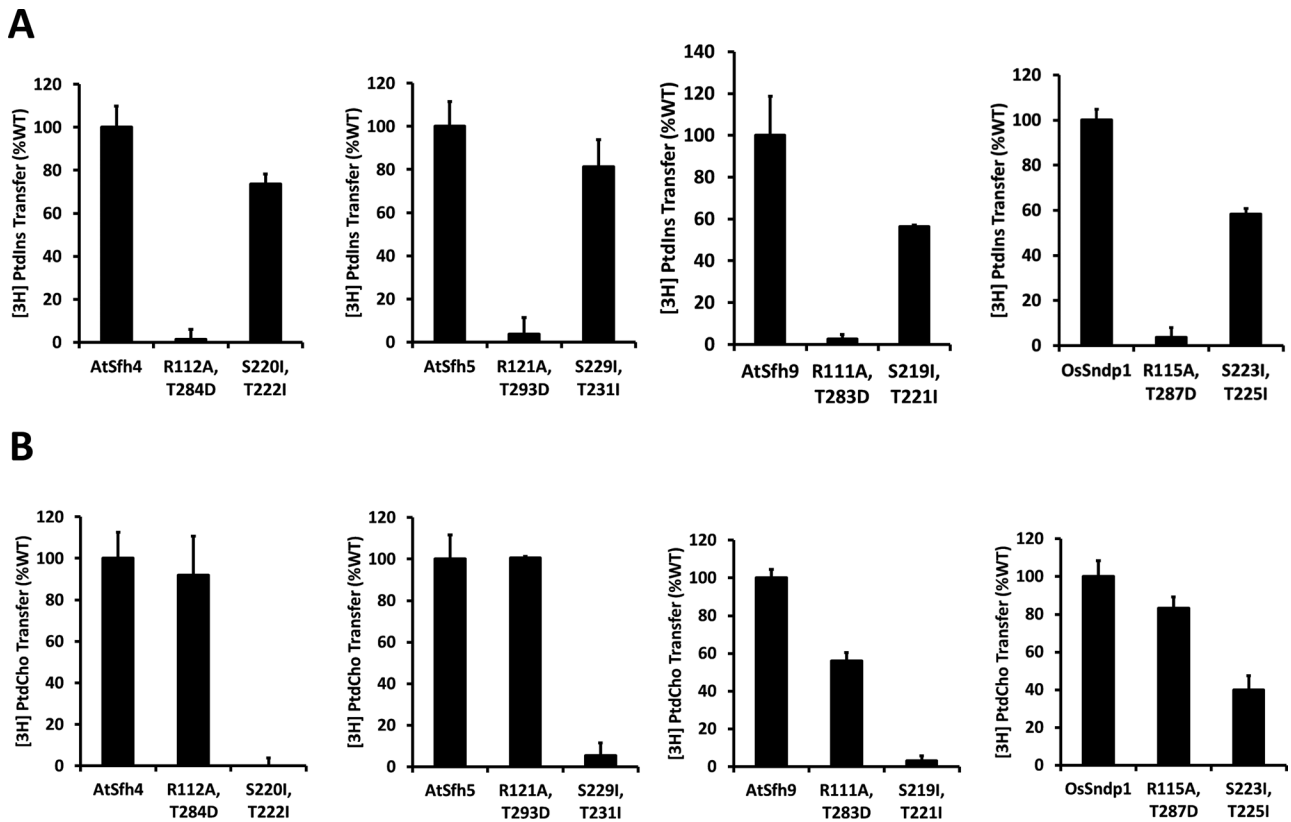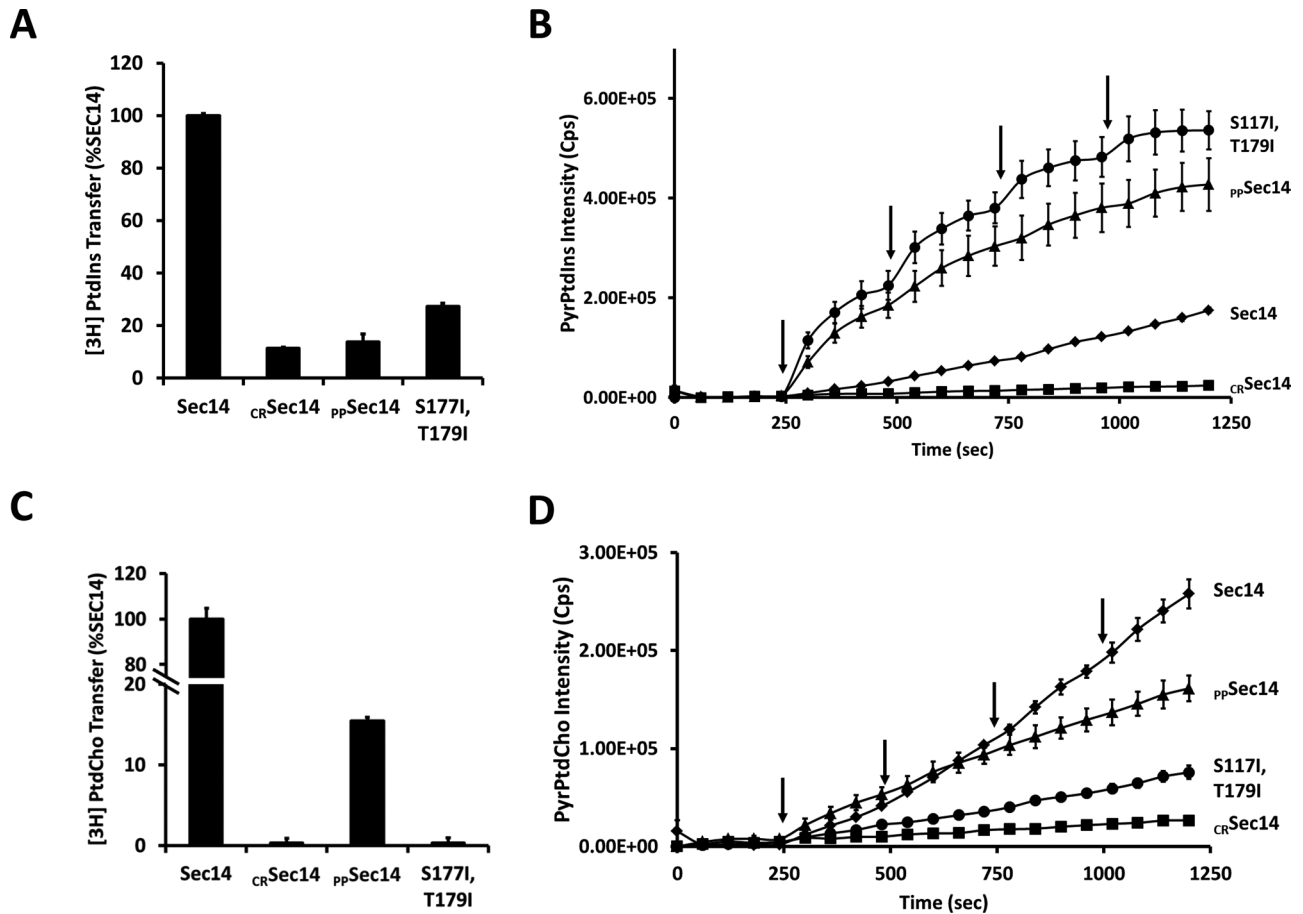
FIGURE 6: Biochemical properties of Sec14-LBDs of Sec14-nodulin proteins. The indicated purified recombinant Sec14-LBDs (10 µg of protein per assay) were assayed for (A) PtdIns- transfer activity using [^{3}H]PtdIns in rat liver microsomes as substrate and PtdCho liposomes as acceptor vesicles and (B) transfer of [^{14}C]PtdCho from donor liposomes to acceptor bovine heart mitochondria (Schaaf *et al.*, 2008). Transfer efficiencies of the corresponding wild-type LBDs are set at 100%, and the relative transfer activities of the mutants compromised for the PtdIns-binding (RT → AD) and PtdCho-binding barcodes (ST → II) are plotted against that normalizing standard (*n* = 3). The assay statistics regarding efficiencies of transfer and assay backgrounds for all proteins analyzed are reported for PtdIns transfer in Supplemental Table S2 and for PtdCho transfer in Supplemental Table S3.

AtSfh1, each of these LBDs also represents a PtdIns- and PtdCho-exchange module that promotes phosphoinositide synthesis built around heterotypic PtdCho/PtdIns exchange. To examine this possibility, we characterized the LBDs of OsSNDP1, AtSfh4, AtSfh5, and AtSfh9 in greater detail. Those representatives not only covered the range of homologies to yeast Sec14 in the *Arabidopsis* Sec14-nodulin protein family, but they also spanned all three classes of Sec14-nodulin proteins (Vincent *et al.*, 2005; Ghosh *et al.*, 2015). Moreover, the rice protein queried the conservation of Sec14-like LBD function in a flowering monocotoledenous plant that is evolutionarily diverged from the flowering dicotyledonous *Arabidopsis*. Sec14-like proteins from the "knockout" moss *Physcomitrella patens* (PPSec14) and the green alga *Chlamydomonas reinhardtii* (CRSec14) represented Sec14-superfamily members from primitive plant models that exhibit either degenerate or otherwise unrecognizable PtdIns-and/or PtdCho-binding barcodes.

Indeed, expression of the Sec14 domains of AtSfh4, AtSfh5, AtSfh9, and OsSNDP1 rescued viability of *sec14-1ts* yeast at the restrictive temperature of 37°C, and, in each case, these activities required a functional PtdIns- and PtdCho-binding barcode (Figure 5B). By contrast, neither expression of PPSec14 (degenerate PtdIns-binding barcode and a recognizable PtdCho-binding barcode) nor that of CRSec14 (lacks recognizable PtdIns or PtdCho-binding barcodes) was sufficient to restore growth to *sec14-1ts* yeast at 37°C

(Figure 5B). The phenotypic results were confirmed by biochemical experiments. Sec14 domains of AtSfh4, AtSfh5, AtSfh9, and OsSNDP1 all exhibited both PtdIns- and PtdCho-transfer activities in vitro, and, in each case, those activities required that the cognate phospholipid-binding barcodes be intact (Figure 6, A and B).

Relative to Sec14, recombinant PPSec14 reproducibly showed low-grade PtdIns-transfer and PtdCho-transfer activities when assayed in the conventional phospholipid-transfer systems (Figure 7, A and C). CRSec14 was devoid of both PtdIns- and PtdCho-transfer activity in those systems (Figure 7, A and C). As independent confirmation of the radiolabeled phospholipid transfer data, we assayed the PPSec14 and CRSec14 proteins in more sensitive fluorescence dequenching PtdIns- and PtdCho-transfer systems. In those assays, transfer is scored by increased fluorescence of phospholipid substrate (labeled with a pyrene-fatty acid at the sn-2 position) upon its transfer from donor vesicles loaded with quencher (2,4,6-trinitrophenylphosphatidylethanolamine [TNP-PtdEtn]) to acceptor vesicles devoid of TNP-PtdEtn (see *Materials and Methods*). Recombinant PPSec14 showed robust transfer activity when pyrene-labeled PtdIns was used as transfer substrate, and this activity was indifferent to amino acid substitutions in the PtdCho-binding barcode (Figure 7B). Of interest, PPSec14 was a better transfer protein than Sec14 in this assay, and our interpretation of that result is that PPSec14 more readily accommodates the bulky pyrene-labeled PtdIns substrate

FIGURE 7: Biochemical properties of Sec14-like proteins of primitive plants. (A) PtdIns-transfer activities of Sec14, $_{CR}$Sec14, $_{PP}$Sec14, and $_{PP}$Sec14^{S177I,T179I} (10 μg of protein per assay) were measured using [^{3}H]PtdIns in rat liver microsomes as substrate and PtdCho liposomes as acceptor vesicles (Bankaitis *et al.*, 1990; Schaaf *et al.*, 2008). Transfer efficiency of Sec14 is set at 100%, and the relative transfer activities of the plant proteins are plotted against that normalizing standard ($n = 3$). The assay statistics regarding efficiencies of transfer and assay backgrounds for $_{CR}$Sec14, $_{PP}$Sec14, and $_{PP}$Sec14^{S177I,T179I} are reported for PtdIns transfer in Supplemental Table S2 and for PtdCho transfer in Supplemental Table S3. (B) Fluorescence intensity of pyrene-PtdIns is plotted as a function of time. Black arrows identify points at which a 1-μg increment of the indicated protein was added. After protein addition, the observed increase in fluorescence intensity is directly proportional to the relative transfer efficiency of the protein being assayed. The initial slope after each addition was calculated to obtain relative transfer efficiency values. For the error bars, $n = 2$. (C) As for A, except that transfer of [^{14}C]PtdCho from donor liposomes to acceptor bovine heart mitochondria is followed (Schaaf *et al.*, 2008). (D) As for B, except that fluorescence intensity of pyrene-PtdCho is followed.

than does Sec14. $_{PP}$Sec14 also exhibited significant PtdCho-transfer activity in this dequenching assay, and this activity was reduced by missense substitutions that alter $_{PP}$Sec14 PtdCho-binding barcode residues (Figure 7D). Again, in both sets of dequenching assay systems, $_{CR}$Sec14 failed to exhibit significant PtdIns- or PtdCho-transfer activity (Figure 7, B and D).

DISCUSSION

Here we demonstrate that the AtSfh1 Sec14 domain has an intrinsic ability to stimulate PtdIns 4-OH kinase activities in a heterologous yeast system and that this function requires the Sec14 domain to harbor both PtdIns- and PtdCho-binding activities. The biological importance of the PtdIns/PtdCho-binding/exchange activities was demonstrated by our finding that ablation of either PtdIns- or Ptd-Cho-binding activity rendered AtSfh1 nonfunctional in generating tip-directed PtdIns(4,5)P$_2$ gradients in growing root hairs and in supporting the polarized membrane growth program required for

proper root hair tip growth. Taken together, the data demonstrate that the two-ligand priming mechanism for potentiated phosphoinositide synthesis described for *Saccharomyces* Sec14 is not limited to yeast but is a conserved feature of Sec14-like PtdIns- and PtdCho-exchange proteins of the most evolutionarily advanced plants. This conservation is remarkable. One possibility is that it represents a convergence of independent evolutionary paths on a two-ligand PtdIns/PtdCho-exchange mechanism for stimulated PtdIns(4)P synthesis. Alternatively, this solution might represent the outcome of lateral transfer of the appropriate genetic module from a fungal pathogen to higher plants and exploitation of that module by higher plants via gene amplification followed by biochemical and functional diversification.

Because x-ray crystallography studies define structural barcodes for PtdIns and PtdCho binding for Sec14 that are written at the primary sequence level, it is now possible to infer certain lipid-binding specificities of biochemically uncharacterized plant Sec14-like
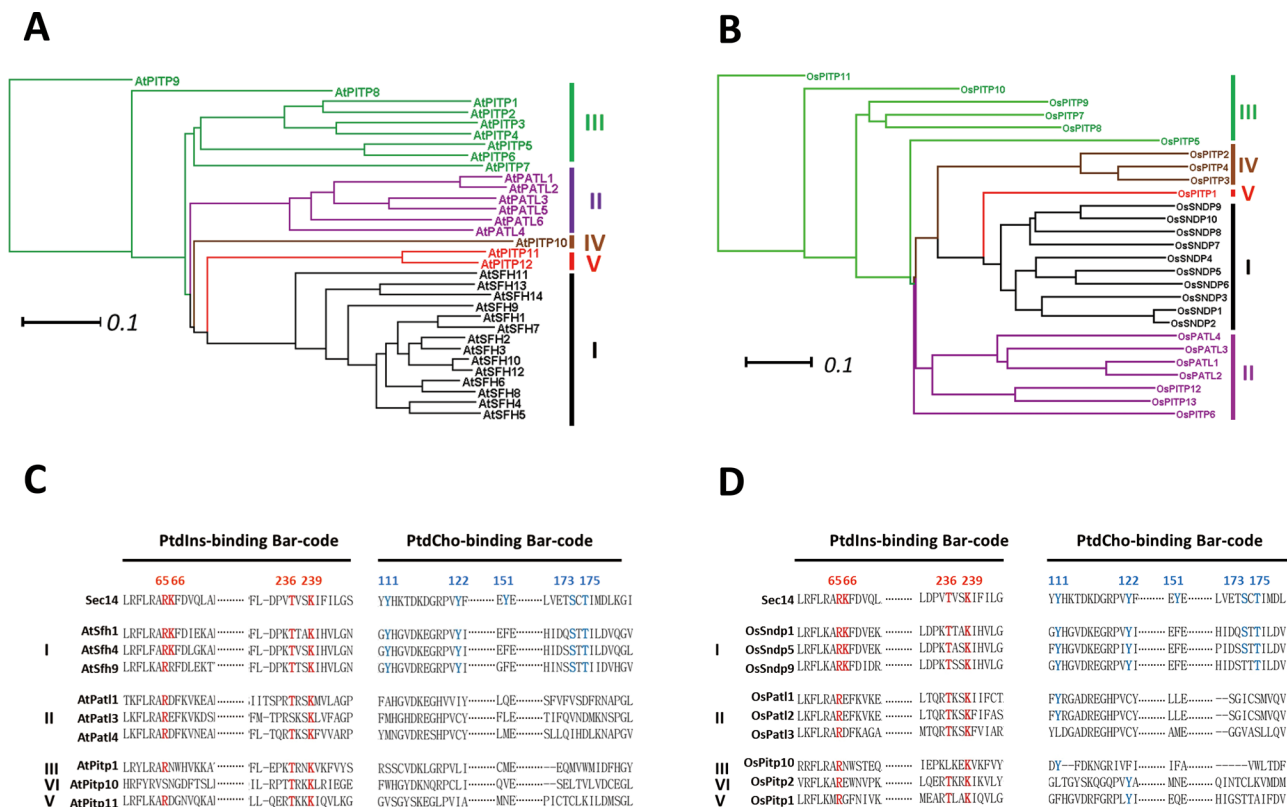
FIGURE 8: Diversification of higher-plant Sec14 domains. Phylogenetic classification of *Arabidopsis* (A) and rice (B) Sec14-LBDs by neighbor joining. Primary sequences were aligned (Clustal Omega, www.ebi.ac.uk/Tools/msa/clustalo/; default parameters with the exception that order = input), and alignments were processed using the ClustalW2 phylogeny tool (www.ebi.ac.uk/Tools/phylogeny/clustalw2_phylogeny/). SplitsTree4 was used to plot and edit phylogenetic trees. For both the *Arabidopsis* and the rice analyses, the Sec14 domains were classified into five clades designated groups I –V, and the different clades are differentiated by color. Bars, 0.1 represents amino acid genetic change of 0.1 (www.ebi.ac.uk/Tools/phylogeny/clustalw2_phylogeny/). The indicated Sec14-LBDs from *Arabidopsis* (C) and rice (D) were aligned using ClustalW2. Conserved PtdIns-binding barcode residues (exemplified by Sec14 $R_{65}T_{236}$ and $K_{66}K_{239}$) and PtdCho-binding barcode residues ($Y_{111}Y_{122}Y_{151}S_{173}T_{175}$) are highlighted in red and blue, respectively.

proteins and domains (Schaaf *et al.*, 2008; Ren *et al.*, 2014). Even a restricted application of this approach to Sec14-like proteins of flowering plants reveals an intriguing pattern. Using the dicot *Arabidopsis* (32 Sec14-like proteins) and the monocot rice (28 Sec14-like proteins) as case models, we observe that the Sec14-like proteins/domains of those corresponding species distribute themselves into five distinct clades in each case (Figure 8, A and B, respectively). Whereas the Sec14-like proteins/domains of these plants generally present well-conserved PtdIns-binding barcodes, the PtdCho-binding barcode is strategically conserved. The inference we draw from such primary sequence comparisons is that the Sec14-like proteins of these plants uniformly preserve their ability to bind PtdIns or some derivative of that phospholipid (e.g., a phosphoinositide). By contrast, the PtdCho-binding barcode is a surprisingly exclusive feature of the Sec14-nodulin proteins, suggesting that these two-domain proteins are evolutionarily engineered to stimulate phosphoinositide synthesis in response to PtdCho metabolic cues. The genetic and biochemical data reported here provide direct experimental support for this idea, and inspection of Sec14-nodulin domain protein sequences from other angiosperms suggests that this is a consistent theme.

Divergences in the second-ligand binding barcode of Sec14-like proteins are proposed to constitute a "front-end" sensing mecha-

nism for integrating the metabolism of diverse lipids/lipophilic molecules with stimulated phosphoinositide synthesis and signaling (Schaaf *et al.*, 2008; Bankaitis *et al.*, 2010; Grabon *et al.*, 2015). The form of this design strategy becomes more apparent when it is incorporated into multidomain protein units. Such molecular contexts enable a tight channeling of newly synthesized phosphoinositide, whose production is primed by dedicated metabolic cues, directly to privileged cohorts of effectors. The notion of such a tightly integrated signaling "pixel" has been described in detail for AtSfh1 (Ghosh *et al.*, 2015; Huang *et al.*, 2016). The PtdIns 4-OH kinase PI-4Kβ1 and the PtdIns(4)P 5-OH kinase PIP5K3 represent the most likely lipid kinases for AtSfh1 interaction, and downstream effectors (while unknown) could (based on purely genetic arguments) include the Agd1 ADP-ribosylation-factor GTPase-activating protein (Preuss *et al.*, 2006; Kusano *et al.*, 2008; Yoo *et al.*, 2012). This is an attractive notion, given the established functional interactions between Sec14 and endosomal ADP-ribosylation-factor GTPase-activating proteins in yeast (Yanagisawa *et al.*, 2002).

Does this concept translate to other multidomain Sec14-like proteins, such as the Sec14-GOLD patellins (Peterman *et al.*, 2004, 2006)? Like the Sec14-nodulins, the patellins are evolutionarily late additions to the plant cohort of Sec14-like proteins, and, as is the case with Sec14-nodulin proteins, the patellin Sec14-domains also

distribute into exclusive phylogenetic clades in both *Arabidopsis* and rice (Figure 8, A and B). In neither case, however, do patellin Sec14-domains exhibit functional PtdCho-binding barcodes (Figure 8C,D). Indeed, using as a guide structural characterizations of PtdCho barcode properties of yeast Sec14-like proteins (Schaaf *et al.*, 2008), the divergence of patellin sequences from the consensus barcode is such that PtdCho binding is almost certainly disqualified for these proteins. Because GOLD domains are advertised to represent protein–protein interaction modules (Anantharaman and Aravind, 2002), it is an attractive hypothesis that patellins promote phosphoinositide synthesis in response to unique sets of second-ligand priming cues and channel newly synthesized phosphoinositide directly to their own privileged sets of downstream effectors. That patellins bind phosphoinositides with some positional specificity supports this basic proposition (Peterman *et al.*, 2004). Of interest, Sec14-GOLD proteins are also expressed outside the plant kingdom, and these too are later evolutionary arrivals, as the non-plant Sec14-GOLD proteins are produced by metazoans but not by unicellular eukaryotes (Anantharaman and Aravind, 2002; Zingg, 2015).

Finally, regardless of whether conservation of PtdIns- and PtdCho-binding barcodes in Sec14-nodulins reflects convergence of independent evolutionary paths on a two-ligand PtdIns/PtdCho-exchange mechanism for stimulated PtdIns(4)P synthesis or exploitation by higher plants of lateral gene transfer from a fungal pathogen, it raises interesting issues. Clearly, the data report a significant biological benefit that comes with a two-ligand PtdIns/PtdCho-exchange strategy for stimulated PtdIns(4)P synthesis. Although we interpret this as a core mechanism for integrating the lipid metabolome with phosphoinositide signaling, a "PtdCho-priming" concept raises the question of why such an abundant membrane lipid might be used as priming ligand. A PtdCho-sensing model seems to be a deaf regulatory instrument based on simple stoichiometric grounds. One possibility is that bulk membrane PtdCho is not generally accessible to (is sequestered from?) Sec14-like PtdIns-/PtdCho-transfer proteins. Perhaps these PITPs can access only restricted pools of PtdCho—for example, newly synthesized PtdCho at the very sites where lipid biosynthetic machineries are located. Such spatial restriction would ensure that the PITP is a direct sensor of PtdCho metabolism. The specific functional relationship between Sec14 and PtdCho synthesis via the cytidine-diphosphate (CDP)-choline pathway in yeast provides a compelling example of the metabolic pathway specificity that can be embedded in such a system (Cleves *et al.*, 1991; Schaaf *et al.*, 2008; Bankaitis *et al.*, 2010). Of perhaps most importance, these outstanding issues highlight additional, and poorly understood, layers of complexity in the rules that license peripheral membrane protein interactions with membrane surfaces for lipid signaling purposes.

MATERIALS AND METHODS

AtSfh1 Sec14-domain homology modeling and MD simulation
Templated homology modeling of the AtSfh1 Sec14 domain and MD simulations of the AtSfh1 LBD bound to PtdIns and PtdCho was performed using the Desmond Molecular Dynamics Package (from Schrödinger [www.schrodinger.com/Desmond/] and D. E. Shaw Research [www.deshawresearch.com/resources_desmond.html]). Optimized homology models were used as starting structures for all atom MD simulations, using explicit water molecules. The OPLS2005 force field as implemented in the Desmond package was used to describe all atoms in the system. Periodic boundary conditions were set using an orthorhombic box with a 12-Å buffer to the edge. The

complex was solvated with the TIP3P water molecules, which were compatible with OPLS parameterization. Physiological salt concentration was fixed to 150 mM by adding custom Na^+ and Cl^- counterions to neutralize the total charge on the system. The system was set at a temperature of 300 K at 1 bar of atmospheric pressure. A series of predefined energy minimization and equilibration steps was carried out to thoroughly relax and equilibrate the system before final 50-ns production runs were executed at NPT ensemble conditions. Post–MD simulation analyses used the Simulation Interaction Diagram (SID) protocol as implemented in the Schrödinger package.

Lipid reagents and synthesis
The L-α-PtdCho and L-α-phosphatidic acid from chicken egg were of highest available quality and were purchased from Avanti Polar Lipids (Alabaster, AL) and used without further purification. 1-Palmitoyl-2-decapyrenyl-*sn*-glycero-3-phosphocholine (PyrPtdCho) was synthesized from 1-palmitoyl-2-hydroxy-*sn*-glycero-3-phosphocholine (Avanti Polar Lipids) and parinaroyl anhydride (Salinger and Lapidot, 1966; Gupta *et al.* 1977) and purified by reverse- phase high-performance liquid chromatography using a Beckman Ultrasphere ODS outfitted with a 4.6 × 25–cm column (Patton *et al.* 1982). 1-Palmitoyl-2-decapyrenyl-*sn*-glycero-3-phosphoinositol (PyrPtdIns) was prepared from yeast PtdIns and parinaroyl anhydride as described (Somerharju and Wirtz, 1982). TNP-PtdEtn was prepared as described by Gordesky and Marinetti (1973) and purified by silica gel column chromatography. Stock solutions of lipids were prepared in methanol and kept at −20°C. The concentrations of PyrPtdIns and PyrPtdCho were determined spectroscopically, and the concentrations of L-α-PtdCho, L-α-phosphatidic acid, and TNP-PtdEtn solutions were determined by the method of Rouser *et al.* (1970). All lipid solutions were taken to ambient temperature before use. All other chemicals used were of highest available quality, and the organic solvents were of spectroscopic grade.

Yeast strains and methods
Strains used were wild-type yeast CTY182 (*MATa ura3-52 lys2-801 Δhis3-200*), CTY1-1A (*MATa ura3-52 lys2-801 Δhis3-200, sec14-1^ts*), and CTY100 (*MATa ura3-52 Δhis3-200 lys2-801 sec14-1^ts sac1-26^cs*). Yeast media and transformation, genetic manipulations, yeast complementation assays, and phosphoinositide measurements have been described in detail (Guo *et al.*, 1999; Rivas *et al.*, 1999; Vincent *et al.*, 2005).

Plant material, growth conditions, and transformation
Arabidopsis thaliana ecotype Columbia was used for all experiments. Methods for plant growth and transformation are detailed in Ghosh *et al.* (2015). Briefly, seeds were plated in 0.8% (wt/vol) top agar (low-melt agarose in 1× Murashige and Skoog Salt and Vitamin Mixture [MS; Gibco BRL, Grand Island, NY]). Seedlings were stratified at 4°C for 4 d and grown vertically under constant light (90 μM m^{-2} s^{-1}) at 22°C for 3–10 d as appropriate. *Atsfh1^{0/0}* null mutant plants (*Atsfh1::T-DNA* line of *A. thaliana* [Brassica family, Columbia ecotype]) were previously described; Vincent *et al.*, 2005). Transgenic plants were generated using *Agrobacterium tumefaciens*–mediated transformation (Clough and Bent, 1998). The transformed seedlings were selected for hygromycin resistance (50 mg/l).

Site-directed mutagenesis
Site-directed mutagenesis was performed according to the protocol from the QuikChange XL Site-Directed Mutagenesis Kit (Stratagene, La Jolla, CA). The cDNAs encoding the appropriate LBDs were

cloned into a yeast centromeric plasmid derived from YCplac33. This plasmid DNA was used as a template to perform site-directed mutagenesis to generate the appropriate LBD mutants. The YCplac33 constructs carried expression cassettes in which transcription of each WT and mutant LBD open reading frame (ORF) was driven by the *SEC14* promoter and subject to *SEC14* termination signals. The plant transformation constructs *Atsfh1^{K96AK271A}*, *Atsfh1^{R96AT268D}*, and *Atsfh1^{S204IT206I}* were generated by site-directed mutagenesis using a plant BAC chromosome carrying *ATSFH1* inserted into an *Escherichia coli*/*Agrobacterium*/plant pCAMBIA shuttle vector obtained from the *Arabidopsis* Biological Resource Center (Ohio State University, Columbus, OH; Vincent *et al.*, 2005).

Expression and purification of recombinant proteins

SEC14 and the appropriate LBD ORF sequences were subcloned into the bacterial expression vector pET28b (Novagen, Madison, WI) for expression of octahistidine-tagged recombinant proteins. These proteins were expressed in *E. coli* BL21-CodonPlus (DE3)-RIL cells (Stratagene). Purification and quantification of these proteins were as described (Schaaf *et al.*, 2008).

Microscopy and imaging

ESEM used living seedlings mounted in 0.8% (wt/vol) top agar visualized with an ESEM TMP instrument (FEI Quanta 200 Field Emission Gun [FEI, Hillsboro, OR]). Confocal microscopy was done on a confocal spinning-disk microscope (Olympus DSU; 100× oil immersion lens [Olympus, Tokyo, Japan]). We performed confocal and Nomarski microscopy on 3-d-old seedlings mounted in water and covered with number 1.5 coverslips. Fluorescence was scanned with an inverted spinning-disk confocal microscope (Olympus DSU; 60x/1.2 numerical aperture oil immersion lens). For each experiment, seven different seedlings were analyzed and <2 root hairs were imaged for each seedling.

Phospholipid transfer assays

Methods for quantifying [^{3}H]PtdIns transfer from rat liver microsomes to PtdCho liposomes and of [^{14}C]PtdCho from liposomes (98 mol% PtdCho, 2 mol% PtdIns) to bovine heart mitochondria have been reported (Bankaitis *et al.*, 1990; Schaaf *et al.*, 2008; Davison *et al.*, 2012).

PyrPtdCho- and PyrPtdIns-transfer measurements were done using a real-time dequenching assay as described by Somerharju *et al.* (1987) with modification. Two vesicle populations, donor (+TNP-PtdEtn quencher) and acceptor (−TNP-PtdEtn quencher), were prepared as follows. For the acceptor vesicles, stock solutions of egg PtdCho and egg phosphatidic acid were mixed in a 291/9 nmol (97/3 mol%) ratio and dried under a stream of N$_2$. The resulting lipid film was then hydrated with 2 ml of low-phosphate buffer (25 mM Na$_2$HPO$_4$, 300 mM NaCl, pH 7.5) and sonicated on ice for 10 min. For the donor vesicles, stock solutions of egg PtdCho, PyrPtdCho/ PyrPtdIns, and TNP-PtdEtn were mixed in a 4/0.5/0.5 nmol ratio, solvent was evaporated, and the lipid film was resuspended in 10 μl of EtOH. The solution was then injected into the buffer containing the acceptor vesicles. After a 5- to 10-min equilibrium period, the fluorescence intensity (excitation, 346 nm; emission 378 nm) was measured in a time course at 37°C using a Horiba Fluorolog 3 fluorimeter (Horiba, Kyoto, Japan). To measure transfer from donor to acceptor, 1 μg protein was injected every 250 s for a total of four injections. To obtain the relative transfer efficiency, the initial slope after each protein injection was calculated, and the mean slope value for each protein (*n* = 4) was normalized to that calculated for purified Sec14.

REFERENCES

Anantharaman V, Aravind L (2002). The GOLD domain, a novel protein module involved in Golgi function and secretion. Genome Biol 3, research0023.

Balla T (2013). Phosphoinositides: tiny lipids with giant impact on cell regulation. Physiol Rev 93, 1019–1137.

Bankaitis VA, Aitken JR, Cleves AE, Dowhan W (1990). An essential role for a phospholipid transfer protein in yeast Golgi function. Nature 347, 561–562.

Bankaitis VA, Mousley CJ, Schaaf G (2010). The Sec14 superfamily and mechanisms for crosstalk between lipid metabolism and lipid signaling. Trends Biochem Sci 35, 150–160.

Böhme K, Li Y, Charlot F, Grierson C, Marrocco K, Okada K, Laloue M, Nogué F (2004). The *Arabidopsis* COW1 gene encodes a phosphatidylinositol transfer protein essential for root hair tip growth. Plant J 40, 686–698.

Boss WF, Im YJ (2012). Phosphoinositide signaling. Annu Rev Plant Biol 63, 409–429.

Braun M, Baluška F, von Witsch M, Menzel D (1999). Redistribution of actin, profilin and phosphatidylinositol-4,5-bisphosphate in growing and maturing root hairs. Planta 209, 435–443.

Bunney TD, Katan M (2010). Phosphoinositide signalling in cancer: beyond PI3K and PTEN. Nat Rev Cancer 10, 342–352.

Cleves AE, McGee TP, Whitters EA, Champion KM, Aitken JR, Dowhan W, Goebl M, Bankaitis VA (1991). Mutations in the CDP-choline pathway for phospholipid biosynthesis bypass the requirement for an essential phospholipid transfer protein. Cell 64, 789–800.

Cleves AE, Novick PJ, Bankaitis VA (1989). Mutations in the SAC1 gene suppress defects in yeast Golgi and yeast actin function. J Cell Biol 109, 2939–2950.

Clough SJ, Bent AF (1998). Floral dip: a simplified method for *Agrobacterium*-mediated transformation of *Arabidopsis thaliana*. Plant J 16, 735–743.

Davison JM, Bankaitis VA, Ghosh R (2012). Devising powerful genetics, biochemical and structural tools in the functional analysis of phosphatidylinositol transfer proteins (PITPs) across diverse species. Methods Cell Biol 1, 108–249.

Di Paolo G, De Camilli P (2006). Phosphoinositides in cell regulation and membrane dynamics. Nature 443, 651–657.

Ghosh R, de Kampos MKF, Huang J, Hur S, Orlowski A, Yang Y, Tripathi A, Nile AH, Lee H-C, Schäfer H, *et al.* (2015). Sec14-nodulin proteins and the patterning of phosphoinositide landmarks for developmental control of membrane morphogenesis. Mol Biol Cell 26, 1764–1781.

Gordesky SE, Marinetti GV (1973). The asymmetric arrangement of phospholipids in the human erythrocyte membrane. Biochem Biophys Res Commun 50, 1027–1031.

Grabon A, Khan D, Bankaitis VA (2015). Phosphatidylinositol transfer proteins and instructive regulation of lipid kinase biology. Biochim Biophys Acta 1851, 724–735.

Grierson CS, Roberts K, Feldmann KA, Dolan L (1997). The COW1 locus of Arabidopsis acts after RHD2, and in parallel with RHD3 and TIP1, to determine the shape, rate of elongation, and number of root hairs produced from each site of hair formation. Plant Physiol 115, 981–990.

Guo S, Stolz LE, Lemrow SM, York JD (1999). SAC1-like domains of yeast SAC1, INP52, and INP53 and human synaptojanin encode phosphoinotide phosphatases. J Biol Chem 274, 12990–12995.

Gupta CM, Radhakrishnan R, Khorana HG (1977). Glycerophospholipid synthesis: improved general method and new analogs containing photoactivable groups. Proc Natl Acad Sci USA 74, 4315–4319.

Heilmann I (2009). Using genetic tools to understand plant phosphoinositide signalling. Trends Plant Sci 14, 171–179.

Heilmann M, Heilmann I (2015). Plant phosphoinositides—complex networks controlling growth and adaptation. Biochim Biophys Acta 1851, 759–769.

Huang J, Ghosh R, Bankaitis VA (2016). Sec14-like phosphatidylinositol transfer proteins and the biological landscape of phosphoinositide signaling in plants. Biochem Biophys Acta, doi:10.1016/j.bbalip.2016.03.027.

Huang J, Kim CM, Xuan Y-H, Park SJ, Piao HL, Je BI, Liu J, Kim TH, Kim B-K, Han C-D (2013). OsSNDP1, a Sec14-nodulin domain-containing protein, plays a critical role in root hair elongation in rice. Plant Mol Biol 82, 39–50.

Ile KE, Schaaf G, Bankaitis VA (2006). Phosphatidylinositol transfer proteins and cellular nanoreactors for lipid signaling. Nat Chem Biol 2, 576–583.

Kapranov P, Routt SM, Bankaitis VA, de Bruijn FJ, Szczglowski K (2001). Nodule-specific regulation of phosphatidylinositol transfer protein expression in Lotus japonicus. Plant Cell 13, 1369–1382.

Kearns MA, Monks DE, Fang M, Rivas MP, Courtney PD, Chen J, Prestwich GD, Thiebert AB, Dewey RE, Bankaitis VA (1998). Novel developmentally regulated phosphoinositide binding proteins from soybean whose expression bypasses the requirement for an essential phosphatidylinositol transfer protein in yeast. EMBO J 17, 4004–4017.

Kusano H, Testerink C, Vermeer JE, Tsuge T, Shimada H, Oka A, Munnik T, Aoyama T (2008). The Arabidopsis phosphatidylinositol phosphate 5-kinase PIP5K3 is a key regulator of root hair tip growth. Plant Cell 20, 367–380.

Monteiro D, Liu Q, Lisboa S, Scherer GEF, Quader H, Malhó R (2005). Phosphoinositides and phosphatidic acid regulate pollen tube growth and reorientation through modulation of [Ca^{2+}] and membrane secretion. J Exp Botany 56, 1665–1674.

Munnik T, Nielsen E (2011). Green light for polyphosphoinositide signals in plants. Curr Opin Plant Biol 14, 489–497.

Patton GM, Fasulo JM, Robins SJ (1982). Separation of phospholipids and individual molecular species of phospholipids by high-performance liquid chromatography. J Lipid Res 23, 190–196.

Peterman TK, Ohol YM, McReynolds LJ, Luna EJ (2004). Patellin 1, a novel Sec14-like protein, localizes to the cell plate and binds phosphoinositides. Plant Physiol 136, 3080–3094.

Peterman TK, Sequeira AS, Samia JA, Lunde EE (2006). Molecular cloning and characterization of patellin1, a novel sec14-related protein, from zucchini (Cucurbita pepo). Plant Physiol 163, 1150–1158.

Phillips SE, Sha B, Topalof L, Xie Z, Alb JG, Klenchin VA, Swigart P, Cockcroft S, Martin TF, Luo M, et al. (1999). Yeast Sec14p deficient in phosphatidylinositol transfer activity is functional in vivo. Mol Cell 4, 187–197.

Preuss ML, Schmitz AJ, Thole JM, Bonner HKS, Otegui MS, Nielsen E (2006). A role for the RabA4b effector protein PI-4K β 1 in polarized expansion of root hair cells in Arabidopsis thaliana. J Cell Biol 172, 991–998.

Qin C, Wang X (2002). The Arabidopsis phospholipase D family. Characterization of a calcium-independent and phosphatidylcholine-selective PLDζ1 with distinct regulatory domains. Plant Physiol 128, 1057–1068.

Ren J, Lin CP, Pathak M, Temple BRS, Nile AH, Mousley C, Duncan MC, Eckert D, Leiker TJ, Ivanova PT, et al. (2014). A phosphatidylinositol transfer protein integrates phosphoinositide signaling with lipid droplet metabolism to regulate a developmental program of nutrient stress-induced membrane biogenesis. Mol Biol Cell 25, 712–727.

Rivas MP, Kearns BG, Xi Z, Guo S, Sekar MC, Hosaka K, Kagiwada S, York JD, Bankaitis VA (1999). Pleiotropic alterations in lipid metabolism in yeast sac1 mutants: relationship to "bypass Sec14p" and inositol auxotrophy. Mol Biol Cell 10, 2235–2250.

Rouser G, Fkeischer S, Yamamoto A (1970). A two dimensional thin layer chromatographic separation of polar lipids and determination of phospholipids by phosphorus analysis of spots. Lipids 5, 494–496.

Salinger Z, Lapidot Y (1966). Synthesis of fatty acid anhydrides by reaction with dicyclohexylcarbodiimide. J Lipid Res 7, 174–175.

Schaaf G, Ortlund E, Tyeryar K, Mousley CJ, Ile K, Woolls M, Garrett T, Raetz CRH, Redinbo M, Bankaitis VA (2008). The functional anatomy of PL binding and regulation of PIP homeostasis by proteins of the Sec14-superfamily. Mol Cell 29, 191–206.

Sha B, Phillips SE, Bankaitis VA, Luo M (1998). Crystal structure of the Saccharomyces cerevisiae phosphatidylinositol-transfer protein. Nature 391, 506–510.

Somerharju PJ, van Loon D, Wirtz KW (1987). Determination of the acyl chain specificity of the bovine liver phosphatidylcholine transfer protein. Application of pyrene-labeled phosphatidylcholine species. Biochemistry 26, 7193–7199.

Somerharju P, Wirtz KWA (1982). Semisynthesis and properties of a fluorescent phosphatidylinositol analogue containing a cis-parinaoyl moiety. Chem Phys Lipids 30, 81–91.

Vincent P, Chua M, Nogue F, Fairbrother A, Mekeel H, Xu Y, Allen N, Bibikova TN, Gilroy S, Bankaitis VA (2005). A Sec14p-nodulin domain phosphatidylinositol transfer protein polarizes membrane growth of Arabidopsis thaliana root hairs. J Cell Biol 168, 801– 812.

Yanagisawa L, Marchena J, Xie Z, Li X, Poon PP, Singer R, Johnston G, Randazzo PA, Bankaitis VA (2002). Activity of specific lipid-regulated ARFGAPs is required for Sec14p-dependent Golgi secretory function in yeast. Mol Biol Cell 13, 2193–2206.

Yang Z (2008). Cell polarity signaling in Arabidopsis. Annu Rev Cell Dev Biol 24, 551–575.

Yoo CM, Quan L, Cannon AE, Wen J, Blancaflor EB (2012). AGD1, a class 1 ARF-GAP, acts in common signaling pathways with phosphoinositide metabolism and the actin cytoskeleton in controlling Arabidopsis root hair polarity. Plant J 69, 1064–1076.

Zingg JM (2015). Vitamin E: a role in signal transduction. Annu Rev Nutr 35, 135–173.